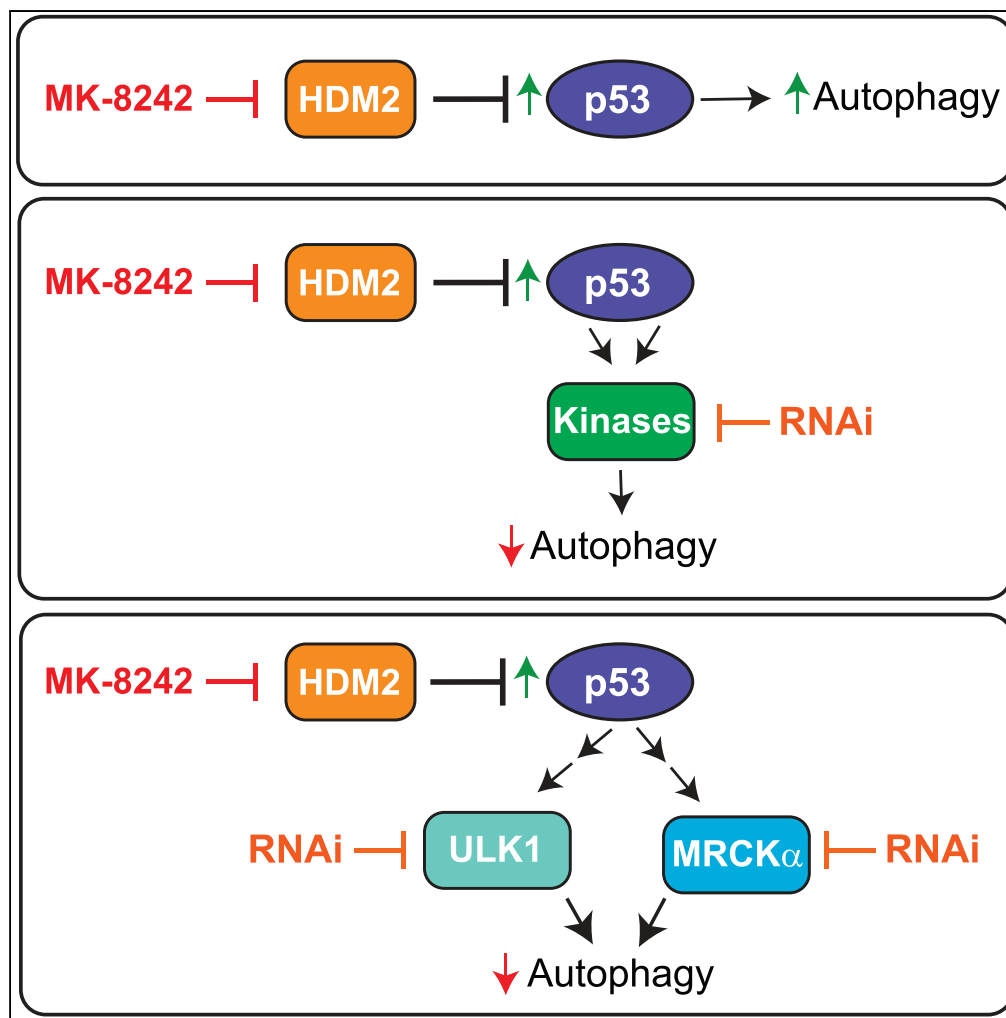**Article**

Identification of Kinases Responsible for p53-Dependent Autophagy

Stephanie L.
Celano, Lisette P.
Yco, Matthew G.
Kortus, ..., Katie R.
Martin, Stuart D.
Shumway, Jeffrey
P. MacKeigan

mackeig1@msu.edu

HIGHLIGHTS

HDM2 inhibitors stabilize
and activate p53 leading
to robust autophagy
induction

RNAi screen uncovers
kinases involved in p53-
dependent autophagy

ULK1 and the actin
cytoskeleton kinase
MRCKα mediate p53-
induced autophagy

Article

Identification of Kinases Responsible for p53-Dependent Autophagy

Stephanie L. Celano,[1,2] Lisette P. Yco,[1,3] Matthew G. Kortus,[2] Abigail R. Solitro,[4] Hakan Gunaydin,[5] Mark Scott,[6] Edward Spooner,[7] Ronan C. O'Hagan,[7] Peter Fuller,[8] Katie R. Martin,[1,2] Stuart D. Shumway,[7] and Jeffrey P. MacKeigan[1,2,4,9,*]

SUMMARY

In cancer, autophagy is upregulated to promote cell survival and tumor growth during times of nutrient stress and can confer resistance to drug treatments. Several major signaling networks control autophagy induction, including the p53 tumor suppressor pathway. In response to DNA damage and other cellular stresses, p53 is stabilized and activated, while HDM2 binds to and ubiquitinates p53 for proteasome degradation. Thus blocking the HDM2-p53 interaction is a promising therapeutic strategy in cancer; however, the potential survival advantage conferred by autophagy induction may limit therapeutic efficacy. In this study, we leveraged an HDM2 inhibitor to identify kinases required for p53-dependent autophagy. Interestingly, we discovered that p53-dependent autophagy requires several kinases, including the myotonic dystrophy protein kinase-like alpha (MRCKα). MRCKα is a CDC42 effector reported to activate actin-myosin cytoskeletal reorganization. Overall, this study provides evidence linking MRCKα to autophagy and reveals additional insights into the role of kinases in p53-dependent autophagy.

INTRODUCTION

Autophagy is a self-degradative process that is important for balancing sources of energy in response to limited nutrients or energy stress. This process starts with the nucleation of phagophores, which expand to double-membrane autophagosomes. These vesicles sequester cytosolic components, including damaged organelles and misfolded proteins. Autophagosomes then fuse and deliver cargo to the lysosome to be degraded into metabolites, which cells reuse to synthesize new macromolecules (Dikic and Elazar, 2018). Autophagy is upregulated to promote cell survival during times of stress, including nutrient deprivation. In cancer, the pro-survival function of autophagy contributes to tumor growth under nutrient-deprived conditions and hypoxic microenvironments and also confers resistance to various drug treatments (Amaravadi et al., 2011; Guo et al., 2011; White, 2012; Yang et al., 2011). Given its important role in cancer, autophagy is now considered a promising target to improve the efficacy of many anticancer treatments.

The activity of several oncogenes and tumor suppressors influence autophagy, in particular, the tumor protein 53 (p53, encoded by *TP53*). During acute cellular stress, such as DNA damage, p53 is stabilized and activated to promote cell-cycle arrest, senescence, or apoptosis (Bieging et al., 2014; Junttila and Evan, 2009; Lane, 1992; Vousden and Prives, 2009). The transcriptional activity of p53 is low under normal conditions with tightly controlled protein stability by the E3-ubiquitin ligase, murine double minute 2 (MDM2; HDM2 in humans), which ubiquitinates p53 for proteasome degradation (Kastenhuber and Lowe, 2017).

HDM2 inhibitors have been developed to directly activate the tumor-suppressing activities of wild-type p53 (Chene, 2003; Levine and Oren, 2009). In 2004, Vassilev and colleagues reported the first inhibitors of the HDM2-p53 interaction (Vassilev et al., 2004). These *cis*-imidazoline analogs, termed Nutlins, are potent and selective small molecules that bind the p53-binding pocket of HDM2 and activate p53 in cancer cells. In recent years, additional HDM2 inhibitors have been developed including MK-8242, a small molecule from Merck & Co., Inc., which has shown promise in phase 1 clinical trials (Ravandi et al., 2016; Tisato et al., 2017; Wagner et al., 2017).

Although p53 has been shown to regulate the cell cycle, senescence, and apoptosis, an increasing body of work suggests that p53 can also mediate autophagy. In response to cellular stress, nuclear p53 can

[1]College of Human Medicine, Michigan State University, Grand Rapids, MI 49503, USA

[2]Center for Cancer Cell Biology, Van Andel Research Institute, Grand Rapids, MI 49503, USA

[3]Department of Physiology, Michigan State University, East Lansing, MI 48824, USA

[4]Van Andel Institute Graduate School, Grand Rapids, MI 49503, USA

[5]Department of Modeling & Informatics, Merck & Co., Inc., Boston, MA 02115, USA

[6]Process Research & Development, Gilead Alberta ULC, Edmonton, AB T6S1A1, Canada

[7]Department of Oncology, Merck & Co., Inc., Boston, MA 02115, USA

[8]Discovery Chemistry, Merck & Co., Inc., Boston, MA 02115, USA

[9]Lead Contact

*Correspondence: mackeig1@msu.edu
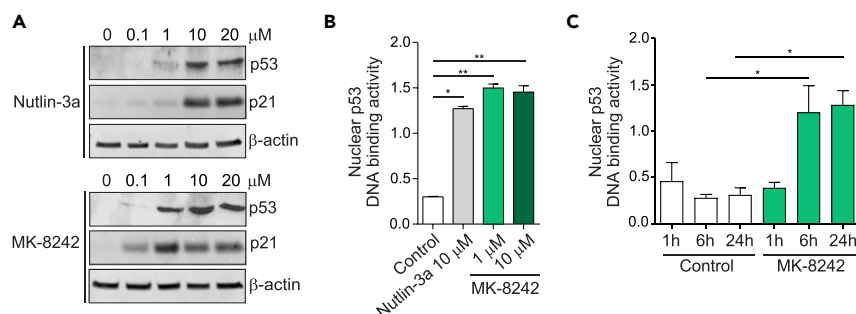
https://doi.org/10.1016/j.isci.2019.04.023

Figure 1. MK-8242 Stabilizes and Activates p53

(A) U2OS cells were treated with HDM2 inhibitors MK-8242 or Nutlin-3a (0, 0.1, 1, 10, and 20 μM) for 24 h and probed for p53, p21, and β-actin. See also Figure S1.

(B) U2OS cells were treated with MK-8242 (1 or 10 μM) or Nutlin-3a (10 μM) for 24 h, nuclear fraction lysates collected, and p53 DNA-binding activity assessed. Bars represent the mean of three biological replicates, and error bars represent standard error of the mean (SEM). One-way ANOVA, Tukey multiple comparison test: *$p < 0.05$, **$p < 0.01$. See also Tables S1 and S2.

(C) U2OS cells were treated with MK-8242 (1 μM) for the indicated times, and nuclear fraction lysates were collected and probed as in (B). Bars represent the mean of three biological replicates, and error bars represent SEM. One-way ANOVA, Tukey multiple comparison test: *$p < 0.05$.

promote autophagy by transcriptionally activating target genes involved in the process, including DNA damage-regulated autophagy modulator 1 (*DRAM1*) (Crighton et al., 2006) and Sestrin 1/2 (*SESN1* and *SESN2*) (Budanov et al., 2002). In contrast, cytoplasmic p53 may inhibit autophagy in a cell-cycle-dependent manner (Tasdemir et al., 2008b, 2008c). In this study, we demonstrate that MK-8242 treatment stabilizes and activates p53 transcriptional activity leading to robust autophagy induction. We further show that well-known autophagy kinase Unc-51-like kinase 1 (ULK1), and lesser-known kinase myotonic dystrophy protein kinase-like alpha (MRCKα, encoded by *CDC42BPA*), are each required for p53-dependent autophagy. We further demonstrate that the regulation of autophagy by p53 does not involve ROCK1/ROCK2, and MRCKα regulation of autophagy is DFCP1 (encoded by *ZFYVE1*) independent, suggesting that MRCKα may regulate autophagosome maturation or turnover.

RESULTS

MK-8242 Stabilizes and Activates p53

To directly compare the cellular potency of MK-8242 to Nutlin-3a, we treated the osteosarcoma cell line U2OS and measured p21 and p53 protein levels by immunoblotting. Nutlin-3a increased p53 and p21 protein expression at 10 μM, whereas MK-8242 increased p53 and p21 at 1.0 μM concentration (Figures 1A and S1). To confirm p21 protein induction was due to p53 stabilization and a subsequent increase in p53 nuclear activity, we measured nuclear p53 bound to double-stranded DNA containing a p53 response element. After 24 h of treatment, nuclear extracts from 1 μM MK-8242-treated cells showed a significant increase in DNA-binding activity when compared with vehicle control-treated samples (Figure 1B). The same result was observed with 10 μM Nutlin-3a treatment, a 10-fold higher concentration. Furthermore, an increase in DNA-binding activity was detected within 6 h of MK-8242 treatment and maintained at 24 h (Figure 1C). To confirm p53 was acting on transcriptional targets within the nucleus, we measured the expression of well-known genes related to p53 signaling using RT-PCR. MK-8242 treatment increased the expression of p53 target genes *CDKN1A* (*p21*) (el-Deiry et al., 1993; el-Deiry et al., 1995), *BAX* (Miyashita and Reed, 1995; Pierzchalski et al., 1997; Thornborrow et al., 2002), *GADD45A* (Kastan et al., 1992), *MDM2* (Juven et al., 1993; Wu et al., 1993), and *TNFRSF10B* (*DR5*) (Liu et al., 2004; Takimoto and El-Deiry, 2000), an effect that was dampened by p53 knockdown (Table S1). Moreover, 1 μM MK-8242 when compared with 10 μM Nutlin-3a increased the expression of several genes known to promote autophagy, including *DRAM1* (Crighton et al., 2006), *SESN2* (Budanov et al., 2002), *ATG4A* (Fitzwalter et al., 2018; Kenzelmann Broz et al., 2013; Mrakovcic and Frohlich, 2018; van der Vos et al., 2012), and *FOXO3A* (Fitzwalter et al., 2018; Kenzelmann Broz et al., 2013; Mrakovcic and Frohlich, 2018; van der Vos et al., 2012), which were similarly decreased with p53 knockdown (Table S2). Together, these results illustrate that MK-8242 stabilizes p53 and activates signaling at a 10-fold lower concentration than Nutlin-3a.
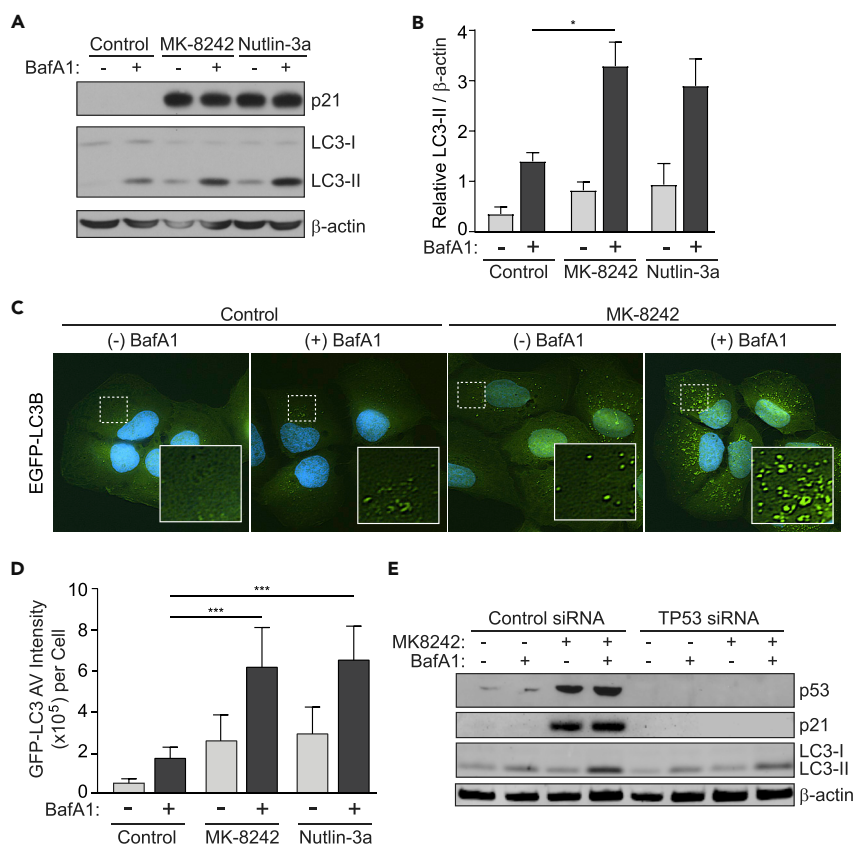
Figure 2. MK-8242 Induces p53-Dependent Autophagy

(A) U2OS cells were treated with MK-8242 (1 μM) or Nutlin-3a (10 μM) for 24 h, with (+) or without (−) BafA1 for the final 1.5 h (total treatment time 24 0068). Lysates were probed for p21, LC3B, and β-actin.

(B) U2OS cells were treated as in (A). Lysates were probed for LC3B and β-actin, and relative LC3B-II signal determined by dividing LC3B-II band intensity by the corresponding β-actin band intensity. Bars represent the mean of three biological experiments, and error bars represent SEM. Two-way ANOVA, Tukey multiple comparison test: *$p < 0.05$.

(C) EGFP-positive puncta (green) were captured in U2OS-EGFP-LC3 cells, treated with MK-8242 (1 μM) with (+) or without (−) BafA1 for the final 1.5 h for a total treatment time of 24 h. Nuclei were counterstained (blue). Insets are a 2× magnification.

(D) U2OS-EGFP-LC3B cells were treated with MK-8242 (1 μM) or Nutlin-3a (10 μM) for 24 h, with (+) or without (−) BafA1 for the final 1.5 h. Images were captured and subjected to intensity quantification (≥ 40 cells per condition). Bars represent the mean intensity of all cells, and error bars represent SEM. One-way ANOVA, Tukey multiple comparison test: ***$p < 0.001$.

(E) U2OS cells treated with control or *TP53* siRNAs for 24 h, and MK-8242 (1 μM) added for an additional 24 h, with (+) or without (+) BafA1 for the final 1.5 h (total treatment time 48 h). Lysates were probed for p53, p21, LC3B, and β-actin. See also Figure S2.

MK-8242 Induces p53-Dependent Autophagy

To determine whether HDM2 inhibition induces autophagy, we used immunoblot analysis and immunofluorescence microscopy to measure microtubule-associated protein 1 light chain 3B (MAP1LC3B; hereafter LC3-II), a protein that associates with autophagic vesicles (AVs) and degrades in lysosomes along with cytosolic cargo. We measure autophagic flux from lysosome-mediated LC3-II turnover. The autophagy field typically measures LC3-II turnover experimentally as LC3-II accumulation in response to treatment with the proton pump inhibitor, bafilomycin A1 (BafA1), which prevents lysosomal degradation (Klionsky et al., 2016; Yamamoto et al., 1998). Autophagic flux increased after 24 h of MK-8242 and Nutlin-3a treatment (Figures 2A and 2B). Furthermore, we observed a significant accumulation of EGFP-LC3B-labeled AVs in MK-8242-treated cells when compared with vehicle control (Figures 2C and 2D). The autophagy induction by HDM2 inhibition could be a direct result of drug activity or a secondary effect related to a general cellular stress response. To delineate this, we tested whether MK-8242-induced autophagy required p53 by
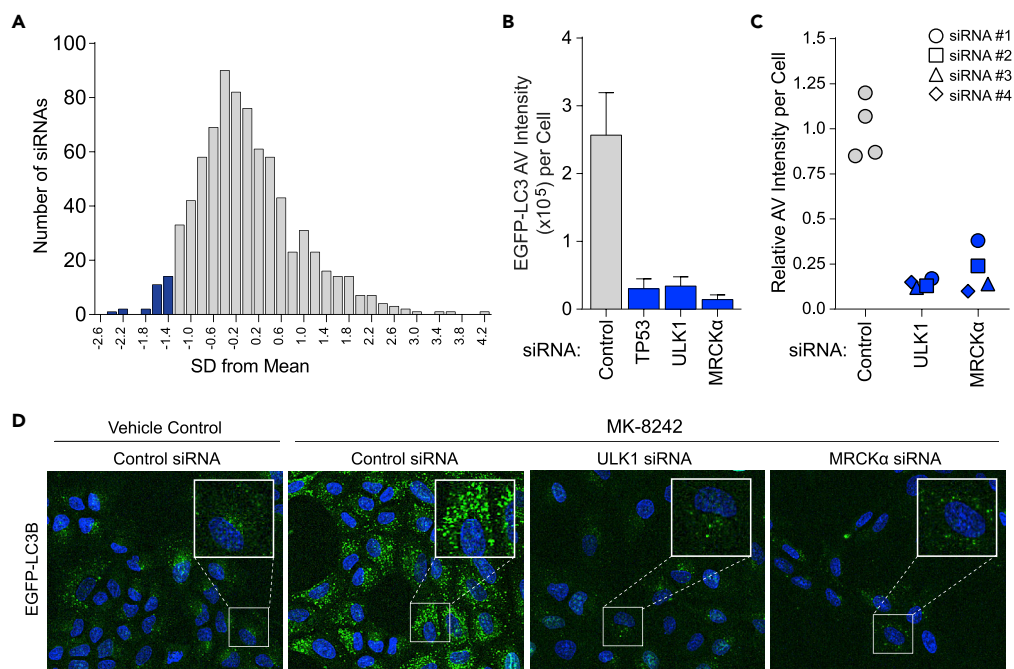
Figure 3. Kinases Mediating p53-Induced Autophagy

(A) U2OS-EGFP-LC3B cells were transfected with a siRNA pool (4 per target gene) for a total of 748 genes. Twenty-four hours post-transfection, cells were treated with MK-8242 with the addition of 100 nM BafA1 for the final hour for a total treatment time of 48 h. siRNAs sorted by standard deviations from plate-normalized means, and bars represent the number of siRNAs within specified standard deviation ranges. See also Table S3.

(B) The top 50 siRNAs determined in (A) subjected to a secondary screen in triplicate. Bars represent the mean intensity per cell for indicated siRNA targets (*TP53*, ULK1, and MRCKα). Error bars represent SEM.

(C) All four siRNAs used in the pool were tested independently for control, ULK1, and MRCKα. Relative EGFP-LC3B-II intensity (AV) per cell for each independent siRNA reported.

(D) U2OS-EGFP-LC3B cells in (A) were treated with MK-8242 and siRNAs targeting ULK1 and MRCKα. Nuclei were counterstained (blue). Insets are at 2× magnification.

measuring LC3-II turnover in cells transfected with *TP53* or non-targeting control small interfering RNAs (siRNAs). In control siRNA-transfected cells, MK-8242 stabilized p53, leading to p21 (*CDKN1A*) induction, and as expected this induction was not affected by BafA1 treatment (Figure 2E). *TP53* knockdown prevented MK-8242-induced stabilization of p53 and p21 induction, as expected, and significantly dampened MK-8242-induced autophagic flux (Figures 2E and S2), thus providing evidence that MK-8242-induced autophagy is p53 dependent.

ULK1 and MRCKα Kinases Mediate p53-Induced Autophagy

Autophagy promotes cell survival and tumor progression in certain contexts; therefore we aimed to identify mediators of p53-induced autophagy. To this end, we completed a confocal microscopy-based siRNA screen of human kinases as well as additional proteins with known roles in autophagy. We transfected cells with siRNAs for 24 h, treated with MK-8242 for 24 h, and treated with BafA1 for the final hour before fixing the cells for microscopy. We quantified EGFP-LC3B-positive AVs and cell counts from confocal images (Figure 3A and Table S3). siRNAs were sorted by standard deviations (SD) from plate-normalized means, and we analyzed the 50 lowest-scoring siRNAs (i.e., most negative SD from the mean) in a secondary screen in triplicate (blue bars in Figure 3A). The siRNAs that significantly decreased AVs in this rescreen included *TP53*, consistent with the p53 dependency observed in Figure 2E, and ULK1, a serine-threonine kinase well known for its essential role in autophagy induction (Figure 3B). Interestingly, knockdown of MRCKα (*CDC42BPA*) also significantly decreased MK-8242-induced AV accumulation. We confirmed the loss of this autophagy phenotype caused by ULK1 and MRCKα knockdown with four independent siRNA sequences (Figure 3C), and the confocal images (Figure 3D) support the autophagy inhibition data (Figure 3B).
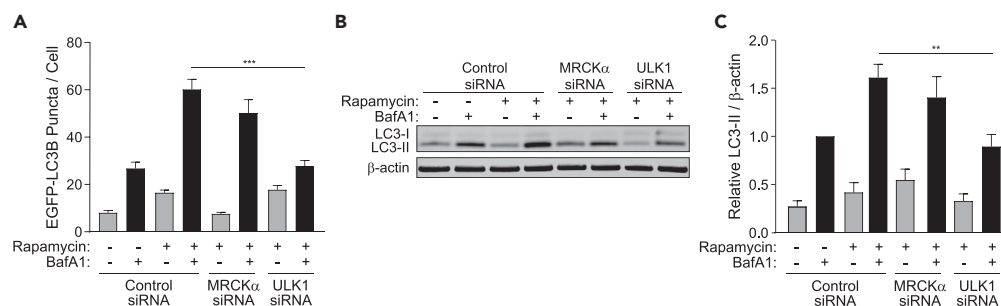
Figure 4. MRCKα Knockdown Does Not Inhibit mTOR-Dependent Autophagy

(A) U2OS-EGFP-LC3B cells were treated with indicated siRNAs for 46 h and rapamycin (100 nM) administered for an additional 2 h, with (+) or without (−) BafA1 for the final 1.5 h for a total treatment time of 48 h. The number of EGFP-LC3B puncta was quantified (≥60 cells per condition). Bars represent means of all cells, and error bars represent SEM. Two-way ANOVA, Tukey multiple comparison test: ***p < 0.001.

(B) U2OS cells were treated with the indicated siRNAs for 46 h, and rapamycin (100 nM) was administered for an additional 2 h, with (+) or without (−) 100 nM BafA1 for the final 1.5 h (total treatment time 48 h). Lysates were probed for LC3B and β-actin as a loading control and imaged by Odyssey (grayscale images shown for all antibodies).

(C) Relative LC3B-II signal from (B) was determined by dividing LC3B-II band intensity by the corresponding β-actin band intensity (normalized to 1.0 for the control siRNA (+) BafA1 condition). Bars represent the mean of three biological replicates, and error bars represent SEM. Two-way ANOVA, Tukey multiple comparison test: **p < 0.01.

See also Figures S3 and S4.

MRCKα Knockdown Does Not Suppress MTORC1-Mediated Autophagy

The nutrient-sensing kinase, mammalian target of rapamycin complex 1 (mTORC1) regulates autophagy (Saxton and Sabatini, 2017). In nutrient-replete conditions, mTORC1 inhibits autophagy induction at the ULK complex (Kim et al., 2011). This autophagy inhibition is relieved upon nutrient starvation or mTORC1 inhibition. Next, we wanted to determine whether MRCKα plays a role in mTORC1-regulated autophagy, in addition to its role in p53-mediated autophagy. To examine whether MRCKα knockdown suppressed mTORC1-dependent autophagy, we measured LC3B-positive AVs in rapamycin-treated cells. ULK1 knockdown significantly decreased rapamycin-induced LC3 turnover, as expected, whereas MRCKα knockdown had minimal to no effect (Figure 4A). To confirm these results, we measured endogenous LC3-II turnover by immunoblot analysis. We treated cells with rapamycin and transfected with siRNAs targeting MRCKα, ULK1, and non-targeting control in the presence or absence of BafA1. Unlike ULK1, MRCKα knockdown did not reduce BafA1-induced LC3-II accumulation in response to rapamycin treatment (Figures 4B and 4C). These results suggest that MRCKα is selectively involved in the regulation of p53-dependent autophagy.

ROCK1/2 Does Not Mediate MK-8242-Induced Autophagy

Rho-associated protein kinase 1 and 2 (ROCK1 and ROCK2) are AGC kinase subfamily members closely related to MRCKα, and these kinases share downstream substrates, for instance, MLC2 (MYL9), MYPT1 (PPP1R12A), and LIMK1 (Kale et al., 2015). Although neither ROCK isoform emerged as a hit in our screen, these proteins have been shown to affect autophagy in certain conditions (Gurkar et al., 2013; Iorio et al., 2010; Mleczak et al., 2013). Accordingly, we wanted to investigate any potential role that they may play in p53-induced autophagy given their similar homology and function to MRCKα. To test this, we measured BafA1-induced LC3B accumulation by fluorescent microscopy and endogenous immunoblotting following siRNA-mediated gene knockdown in U2OS cells treated with MK-8242. To rule out compensatory effects between ROCK isoforms, we targeted both simultaneously by pooling ROCK1 and ROCK2 siRNAs (Riento and Ridley, 2003). We similarly knocked down both MRCKα and its related isoform, MRCKβ, for completeness. In these experiments, we found that dual ROCK1/ROCK2 knockdown did not significantly reduce BafA1-induced LC3-II accumulation during MK-8242 treatment, in contrast to the knockdown of MRCKα/β (Figure S3). To further investigate ROCK1/ROCK2 and MRCKα inhibition pharmacologically, we treated cells with the ROCK inhibitor Y-27632 (Uehata et al., 1997) or the MRCK inhibitor BDP-5290 (Unbekandt et al., 2014). Similar to knockdown, concurrent treatment with MK-8242 and either 1 μM or 10 μM Y-27632 did not alter LC3-II turnover (Figure S4A), whereas treatment with the MRCK inhibitor BDP-5290 decreased LC3-II turnover in a dose-dependent manner (Figure S4B). These data suggest that specifically targeting MRCKα may be sufficient to disrupt p53-dependent autophagy induction by HDM2 inhibitors.
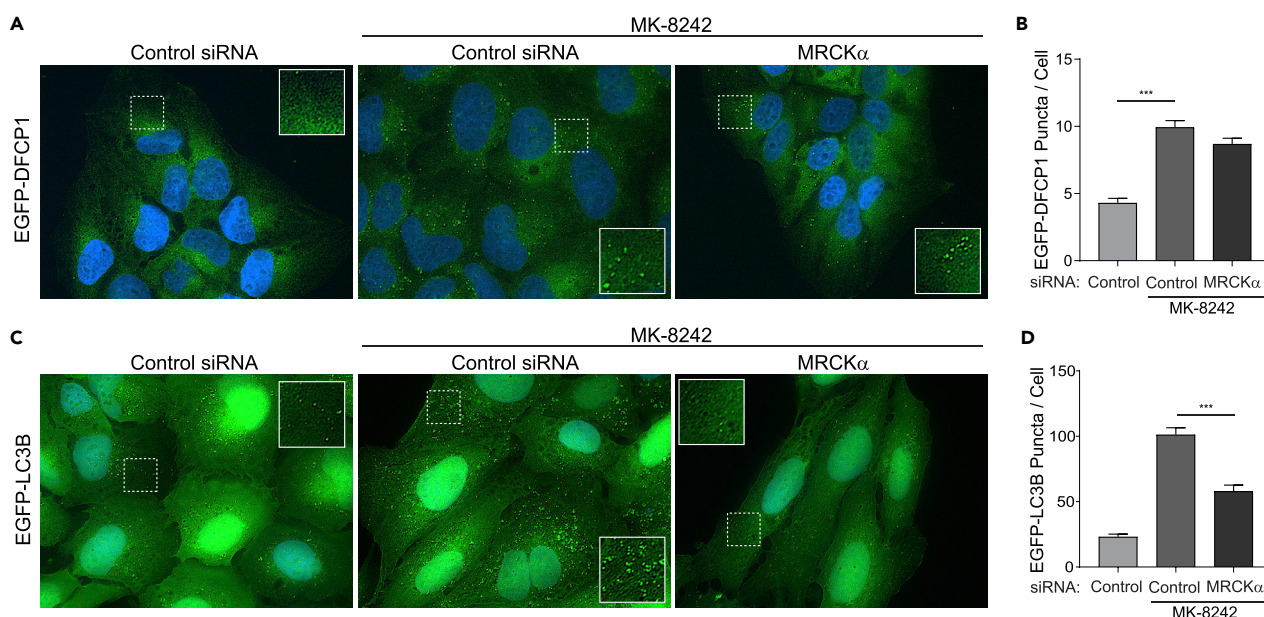
Figure 5. MRCKα Mediates Autophagosome Formation

(A) U2OS cells stably expressing EGFP-DFCP1 were treated with the indicated siRNAs for 24 h, and MK-8242 (1 μM) administered for an additional 24 h for a total treatment time of 48 h. Nuclei were counterstained (blue). Representative 60✕/oil images shown, and insets are a 2✕ magnification. See also Figure S5.

(B) The number of EGFP-DFCP1-positive puncta quantified from the images obtained in (A) (≥50 cells per condition). Bars represent means of all cells, and error bars represent SEM. Two-way ANOVA, Tukey multiple comparison test: ***$p < 0.001$.

(C) U2OS cells stably expressing EGFP-LC3B were treated with indicated siRNAs for 24 h and MK-8242 (1 μM) administered for an additional 24 h, with (+) or without (−) BafA1 for the final 1.5 h for a total treatment time of 48 h. Nuclei were counterstained (blue). Images shown contain 100 nM BafA1. Insets are a 2✕ magnification.

(D) The number of EGFP-LC3B-positive puncta was quantified from the images obtained in (C) (≥50 cells per condition). Bars represent means of all cells, and error bars represent SEM. Two-way ANOVA, Tukey multiple comparison test: ***$p < 0.001$.

MRCKα Mediates Autophagosome Formation

MRCKα is a mediator of p53-dependent autophagy. To elucidate the role of MRCKα in the nucleation and completion stages of autophagy, we measured exogenous markers for nucleation (i.e., DFCP1) and completion (i.e., LC3B) in the context of HDM2 inhibition. We stably expressed the omegasome marker, EGFP-DFCP1, in U2OS cells and monitored DFCP1-positive puncta by fluorescent microscopy (Martin et al., 2018). MK-8242 treatment significantly increased DFCP1 puncta (Figures 5A and 5B), confirming that HDM2 inhibition activated p53-induced autophagy. However, MRCKα knockdown failed to affect DFCP1 puncta levels (Figures 5A and 5B). To verify the effects of MRCKα knockdown in this set of experiments, on the completion stage of autophagy, we again treated EGFP-LC3B-expressing U2OS cells with MK-8242 and either non-targeting control or MRCKα siRNAs. Indeed, MRCKα knockdown significantly decreased LC3B turnover in response to MK-8242 treatment (Figures 5C and 5D). These results suggest that MRCKα is not required for the recruitment and formation of DFCP1-positive structures at the omegasome, but may regulate autophagosome maturation or turnover.

DISCUSSION

Stress signals, including oncogenic activation and DNA damage, activate p53 as a transcription factor, which regulates a large number of target genes critical in cell cycle arrest, senescence, apoptosis, and more recently autophagy. The p53 protein has been reported to have a dual function in autophagy depending on its subcellular localization (Maiuri et al., 2010; Tasdemir et al., 2008a). In this study, we used an HDM2 inhibitor, MK-8242, to uncover additional answers that link p53 to autophagy induction. We first confirmed that MK-8242 is a potent HDM2 inhibitor and induces p53 stabilization, 10-fold over the established HDM2 inhibitor Nutlin-3a. In fact, HDM2 inhibitors using a piperidine scaffold, such as MK-8242, have demonstrated increased potency and bioavailability over original HDM2 inhibitors (Bogen et al., 2016; Pan et al., 2014). We also observed increased gene expression of several autophagy-related p53 target genes, including *DRAM1*, *SESN2*, *ATG4A*, and *FOXO3A* (Table S2) in response to HDM2 inhibition. Importantly,

earlier work supports our results suggesting that autophagy induction is dependent on p53 transcriptional activity (Kenzelmann Broz et al., 2013).

In a report 10 years ago, Tasdemir and colleagues concluded that loss or inhibition of p53 induces autophagy and used p53 mutations in either the nuclear export signal or nuclear localization sequence to conclude that cytoplasmic p53 specifically inhibits autophagy (Tasdemir et al., 2008a). In contrast, our data support the role of nuclear p53 robustly inducing autophagy. Tasdemir and colleagues used several different approaches to inhibit p53, including chemical inhibition (pifithrin-α), p53 knockout cells, and p53 knockdown using siRNAs. Conversely, we used HDM2 chemical inhibition to stabilize and activate p53 and p53 knockdown using siRNAs to inhibit p53. Many compounds are known to induce autophagy as a non-specific or specific endoplasmic reticulum stress response. Moreover, pifithrin-α blocks p53 transcriptional activity, and also other transcription factors and target genes essential for cellular homeostasis, making any conclusions from this compound difficult owing to its lack of specificity (Sohn et al., 2009; Walton et al., 2005). Based on data presented here, we can conclude that HDM2 inhibitors stabilize and activate p53 leading to robust autophagy induction.

Our results also support prior studies that concluded that nuclear p53 can promote autophagy by transcriptionally activating target genes involved in the process, *DRAM1* (Crighton et al., 2006), *SESN2* (Budanov et al., 2002), *ATG4A* (Fitzwalter et al., 2018; Kenzelmann Broz et al., 2013; Mrakovcic and Frohlich, 2018; van der Vos et al., 2012), and *FOXO3A* (Fitzwalter et al., 2018; Kenzelmann Broz et al., 2013; Mrakovcic and Frohlich, 2018; van der Vos et al., 2012). In a landmark publication, Amaravadi and colleagues using a Myc-induced model of lymphoma inhibited autophagy to enhance cell death (Amaravadi et al., 2007). In this Myc-induced model, they also examined p53 and concluded that nuclear p53 promoted apoptotic cell death, while the surviving cells were undergoing autophagy. After autophagy inhibition tumor regression occurred, suggesting that p53-induced autophagy contributes to tumor cell survival.

Our kinome siRNA screen to identify mediators of p53-dependent autophagy highlighted the canonical autophagy regulator, ULK1. Interestingly, our findings also revealed MRCKα as a positive regulator of autophagy. MRCKα is a CDC42 effector protein (Heikkila et al., 2011) that initiates phosphorylation events on MLC2 (Nakamura et al., 2000), MYPT1, MYPT3 (*PPP1R16A*) (Tan et al., 2001; Yong et al., 2006), and LIMK1 (Sumi et al., 2001). MRCKα also cooperates with LRAP25 (*FAM89B*) and LIMK1 to reorganize F-actin for cell protrusion and migration at the trailing end of the cell (Lee et al., 2014). Recent research on MRCK has been closely tied to ROCK1/ROCK2, given shared homology and substrates (Wilkinson et al., 2005; Zhao and Manser, 2015). However, MRCKα activation by PDK1 (*PDPK1*) has been associated with lamellipodia retraction (Gagliardi et al., 2014) and acts independently of ROCK to regulate lamellar actomyosin dynamics (Tan et al., 2008). Our data also support a role for MRCKα in actin dynamics, as cells treated with MRCKα siRNAs and stained for F-actin (phalloidin) display an actin network with well-aligned stress fibers (Figure S5). Moreover, the initiation and trafficking of autophagosomes may depend on actin cytoskeleton signaling proteins (Kast and Dominguez, 2017). Branched actin polymerization is essential for nucleation (Kast and Dominguez, 2015; Kast et al., 2015), whereas actomyosin dynamics is essential for elongation and transport of autophagosomes (Brandstaetter et al., 2014; Cordonnier et al., 2001; Kast and Dominguez, 2017; Miserey-Lenkei et al., 2010; Tang et al., 2011). Here, for the first time, we implicate the actin-myosin regulatory kinase MRCKα not in the assembly of the omegasome (DFCP1), but in autophagosome (LC3-II) formation, thus providing further evidence for the role of actin dynamics in autophagosome structure and expansion (Mi et al., 2015).

MRCKα-targeted inhibition of p53-induced autophagy could be beneficial in many applications related to cancer. Recently, MRCK inhibitors, BDP-8900 and BDP-9066, have been reported (Unbekandt et al., 2018). MRCK expression is elevated in several types of cancer (Unbekandt and Olson, 2014) and associated with poor prognosis in breast cancer (van 't Veer et al., 2002). Additional research with these inhibitors will be required to determine the actual benefit and timing of MRCK and HDM2 inhibitor adjuvant treatment. As others have reported an increase in apoptosis upon Nutlin-3a treatment with autophagy inhibition, future work must determine if inhibiting p53-induced autophagy through MRCKα will sensitize tumor cells to HDM2 inhibition and induce apoptosis (Davaadelger et al., 2017; Sullivan et al., 2015).

Limitations of the Study

We have uncovered a previously unrecognized role for MRCKα in mediating p53-driven autophagy; however, the precise mechanism by which this protein functions in autophagy remains to be determined.

Moreover, our study suggests that MRCKα can be targeted to suppress autophagy induced by HDM2 inhibitors; however, the effects of such a combination strategy *in vivo* and on tumor growth will be the focus of future work.

METHODS

All methods can be found in the accompanying Transparent Methods supplemental file.

SUPPLEMENTAL INFORMATION

Supplemental Information can be found online at https://doi.org/10.1016/j.isci.2019.04.023.

AUTHOR CONTRIBUTIONS

Conceptualization, K.R.M., R.C.O., and J.P.M.; Methodology, S.L.C., L.P.Y, M.G.K., K.R.M., A.R.S., H.G., M.S., E.S., S.D.S., P.F., and J.P.M.; Validation, S.L.C., L.P.Y., M.G.K., K.R.M., and A.R.S.; Formal Analysis, S.L.C., L.P.Y., K.R.M., M.G.K., A.R.S., and J.P.M.; Investigation, S.L.C., L.P.Y, K.R.M., M.G.K., and J.P.M.; Resources, K.R.M., S.L.C., S.D.S., P.F., and J.P.M.; Writing – Original Draft, S.L.C., L.P.Y., and J.P.M.; Writing – Review & Editing, S.L.C., L.P.Y., K.R.M., A.R.S., R.C.O., S.D.S., P.F., and J.P.M.; Visualization, S.L.C., L.P.Y., and J.P.M.; Supervision, K.R.M., S.D.S., P.F., and J.P.M.; Project Administration, R.C.O., S.D.S., P.F., and J.P.M.; Funding Acquisition, R.C.O. and J.P.M.

DECLARATION OF INTERESTS

The authors declare no competing interests.

REFERENCES

Amaravadi, R.K., Lippincott-Schwartz, J., Yin, X.M., Weiss, W.A., Takebe, N., Timmer, W., DiPaola, R.S., Lotze, M.T., and White, E. (2011). Principles and current strategies for targeting autophagy for cancer treatment. Clin. Cancer Res. *17*, 654–666.

Amaravadi, R.K., Yu, D., Lum, J.J., Bui, T., Christophorou, M.A., Evan, G.I., Thomas-Tikhonenko, A., and Thompson, C.B. (2007). Autophagy inhibition enhances therapy-induced apoptosis in a Myc-induced model of lymphoma. J. Clin. Invest. *117*, 326–336.

Bieging, K.T., Mello, S.S., and Attardi, L.D. (2014). Unravelling mechanisms of p53-mediated tumour suppression. Nat. Rev. Cancer *14*, 359–370.

Bogen, S.L., Pan, W., Gibeau, C.R., Lahue, B.R., Ma, Y., Nair, L.G., Seigel, E., Shipps, G.W., Jr., Tian, Y., Wang, Y., et al. (2016). Discovery of novel 3,3-disubstituted piperidines as orally bioavailable, potent, and efficacious HDM2-p53 inhibitors. ACS Med. Chem. Lett. *7*, 324–329.

Brandstaetter, H., Kishi-Itakura, C., Tumbarello, D.A., Manstein, D.J., and Buss, F. (2014). Loss of functional MYO1C/myosin 1c, a motor protein involved in lipid raft trafficking, disrupts autophagosome-lysosome fusion. Autophagy *10*, 2310–2323.

Budanov, A.V., Shoshani, T., Faerman, A., Zelin, E., Kamer, I., Kalinski, H., Gorodin, S., Fishman, A., Chajut, A., Einat, P., et al. (2002). Identification of a novel stress-responsive gene Hi95 involved in regulation of cell viability. Oncogene *21*, 6017–6031.

Chene, P. (2003). Inhibiting the p53-MDM2 interaction: an important target for cancer therapy. Nat. Rev. Cancer *3*, 102–109.

Cordonnier, M.N., Dauzonne, D., Louvard, D., and Coudrier, E. (2001). Actin filaments and myosin I alpha cooperate with microtubules for the movement of lysosomes. Mol. Biol. Cell *12*, 4013–4029.

Crighton, D., Wilkinson, S., O'Prey, J., Syed, N., Smith, P., Harrison, P.R., Gasco, M., Garrone, O., Crook, T., and Ryan, K.M. (2006). DRAM, a p53-induced modulator of autophagy, is critical for apoptosis. Cell *126*, 121–134.

Davaadelger, B., Perez, R.E., Zhou, Y., Duan, L., Gitelis, S., and Maki, C.G. (2017). The IGF-1R/AKT pathway has opposing effects on Nutlin-3a-induced apoptosis. Cancer Biol. Ther. *18*, 895–903.

Dikic, I., and Elazar, Z. (2018). Mechanism and medical implications of mammalian autophagy. Nat. Rev. Mol. Cell Biol. *19*, 349–364.

el-Deiry, W.S., Tokino, T., Velculescu, V.E., Levy, D.B., Parsons, R., Trent, J.M., Lin, D., Mercer, W.E., Kinzler, K.W., and Vogelstein, B. (1993). WAF1, a potential mediator of p53 tumor suppression. Cell *75*, 817–825.

el-Deiry, W.S., Tokino, T., Waldman, T., Oliner, J.D., Velculescu, V.E., Burrell, M., Hill, D.E., Healy, E., Rees, J.L., Hamilton, S.R., et al. (1995). Topological control of p21WAF1/CIP1 expression in normal and neoplastic tissues. Cancer Res. *55*, 2910–2919.

Fitzwalter, B.E., Towers, C.G., Sullivan, K.D., Andrysik, Z., Hoh, M., Ludwig, M., O'Prey, J., Ryan, K.M., Espinosa, J.M., Morgan, M.J., et al. (2018). Autophagy inhibition mediates apoptosis sensitization in cancer therapy by relieving FOXO3a turnover. Dev. Cell *44*, 555–565.e3.

Gagliardi, P.A., di Blasio, L., Puliafito, A., Seano, G., Sessa, R., Chianale, F., Leung, T., Bussolino, F., and Primo, L. (2014). PDK1-mediated activation of MRCKalpha regulates directional cell migration and lamellipodia retraction. J. Cell Biol. *206*, 415–434.

Guo, J.Y., Chen, H.Y., Mathew, R., Fan, J., Strohecker, A.M., Karsli-Uzunbas, G., Kamphorst, J.J., Chen, G., Lemons, J.M., Karantza, V., et al. (2011). Activated Ras requires autophagy to maintain oxidative metabolism and tumorigenesis. Genes Dev. *25*, 460–470.

Gurkar, A.U., Chu, K., Raj, L., Bouley, R., Lee, S.H., Kim, Y.B., Dunn, S.E., Mandinova, A., and Lee, S.W. (2013). Identification of ROCK1 kinase as a critical regulator of Beclin1-mediated autophagy during metabolic stress. Nat. Commun. *4*, 2189.

Heikkila, T., Wheatley, E., Crighton, D., Schroder, E., Boakes, A., Kaye, S.J., Mezna, M., Pang, L., Rushbrooke, M., Turnbull, A., et al. (2011). Co-crystal structures of inhibitors with MRCKbeta, a key regulator of tumor cell invasion. PLoS One *6*, e24825.

Iorio, F., Bosotti, R., Scacheri, E., Belcastro, V., Mithbaokar, P., Ferriero, R., Murino, L., Tagliaferri, R., Brunetti-Pierri, N., Isacchi, A., et al. (2010). Discovery of drug mode of action and drug repositioning from transcriptional responses. Proc. Natl. Acad. Sci. U S A *107*, 14621–14626.

Junttila, M.R., and Evan, G.I. (2009). p53–a Jack of all trades but master of none. Nat. Rev. Cancer *9*, 821–829.

Juven, T., Barak, Y., Zauberman, A., George, D.L., and Oren, M. (1993). Wild type p53 can mediate sequence-specific transactivation of an internal promoter within the mdm2 gene. Oncogene *8*, 3411–3416.

Kale, V.P., Hengst, J.A., Desai, D.H., Amin, S.G., and Yun, J.K. (2015). The regulatory roles of ROCK and MRCK kinases of cancer cell migration. Cancer Lett. *361*, 185–196.

Kast, D.J., and Dominguez, R. (2015). WHAMM links actin assembly via the Arp2/3 complex to autophagy. Autophagy *11*, 1702–1704.

Kast, D.J., and Dominguez, R. (2017). The cytoskeleton-autophagy connection. Curr. Biol. *27*, R318–R326.

Kast, D.J., Zajac, A.L., Holzbaur, E.L., Ostap, E.M., and Dominguez, R. (2015). WHAMM directs the Arp2/3 complex to the ER for autophagosome biogenesis through an actin comet tail mechanism. Curr. Biol. *25*, 1791–1797.

Kastan, M.B., Zhan, Q., el-Deiry, W.S., Carrier, F., Jacks, T., Walsh, W.V., Plunkett, B.S., Vogelstein, B., and Fornace, A.J., Jr. (1992). A mammalian cell cycle checkpoint pathway utilizing p53 and GADD45 is defective in ataxia-telangiectasia. Cell *71*, 587–597.

Kastenhuber, E.R., and Lowe, S.W. (2017). Putting p53 in context. Cell *170*, 1062–1078.

Kenzelmann Broz, D., Spano Mello, S., Bieging, K.T., Jiang, D., Dusek, R.L., Brady, C.A., Sidow, A., and Attardi, L.D. (2013). Global genomic profiling reveals an extensive p53-regulated autophagy program contributing to key p53 responses. Genes Dev. *27*, 1016–1031.

Kim, J., Kundu, M., Viollet, B., and Guan, K.L. (2011). AMPK and mTOR regulate autophagy through direct phosphorylation of Ulk1. Nat. Cell Biol. *13*, 132–141.

Klionsky, D.J., Abdelmohsen, K., Abe, A., Abedin, M.J., Abeliovich, H., Acevedo Arozena, A., Adachi, H., Adams, C.M., Adams, P.D., Adeli, K., et al. (2016). Guidelines for the use and interpretation of assays for monitoring autophagy (3rd edition). Autophagy *12*, 1–222.

Lane, D.P. (1992). Cancer. p53, guardian of the genome. Nature *358*, 15–16.

Lee, I.C., Leung, T., and Tan, I. (2014). Adaptor protein LRAP25 mediates myotonic dystrophy kinase-related Cdc42-binding kinase (MRCK) regulation of LIMK1 protein in lamellipodial F-actin dynamics. J. Biol. Chem. *289*, 26989–27003.

Levine, A.J., and Oren, M. (2009). The first 30 years of p53: growing ever more complex. Nat. Rev. Cancer *9*, 749–758.

Liu, X., Yue, P., Khuri, F.R., and Sun, S.Y. (2004). p53 upregulates death receptor 4 expression through an intronic p53 binding site. Cancer Res. *64*, 5078–5083.

Maiuri, M.C., Galluzzi, L., Morselli, E., Kepp, O., Malik, S.A., and Kroemer, G. (2010). Autophagy regulation by p53. Curr. Opin. Cell Biol. *22*, 181–185.

Martin, K.R., Celano, S.L., Solitro, A.R., Gunaydin, H., Scott, M., O'Hagan, R.C., Shumway, S.D., Fuller, P., and MacKeigan, J.P. (2018). A potent and selective ULK1 inhibitor suppresses autophagy and sensitizes cancer cells to nutrient stress. iScience *8*, 74–84.

Mi, N., Chen, Y., Wang, S., Chen, M., Zhao, M., Yang, G., Ma, M., Su, Q., Luo, S., Shi, J., et al. (2015). CapZ regulates autophagosomal membrane shaping by promoting actin assembly inside the isolation membrane. Nat. Cell Biol. *17*, 1112–1123.

Miserey-Lenkei, S., Chalancon, G., Bardin, S., Formstecher, E., Goud, B., and Echard, A. (2010). Rab and actomyosin-dependent fission of transport vesicles at the Golgi complex. Nat. Cell Biol. *12*, 645–654.

Miyashita, T., and Reed, J.C. (1995). Tumor suppressor p53 is a direct transcriptional activator of the human bax gene. Cell *80*, 293–299.

Mleczak, A., Millar, S., Tooze, S.A., Olson, M.F., and Chan, E.Y. (2013). Regulation of autophagosome formation by Rho kinase. Cell Signal. *25*, 1–11.

Mrakovcic, M., and Frohlich, L.F. (2018). p53-mediated molecular control of autophagy in tumor cells. Biomolecules *8*, 1–18.

Nakamura, N., Oshiro, N., Fukata, Y., Amano, M., Fukata, M., Kuroda, S., Matsuura, Y., Leung, T., Lim, L., and Kaibuchi, K. (2000). Phosphorylation of ERM proteins at filopodia induced by Cdc42. Genes Cells *5*, 571–581.

Pan, W., Lahue, B.R., Ma, Y., Nair, L.G., Shipps, G.W., Jr., Wang, Y., Doll, R., and Bogen, S.L. (2014). Core modification of substituted piperidines as novel inhibitors of HDM2-p53

protein-protein interaction. Bioorg. Med. Chem. Lett. *24*, 1983–1986.

Pierzchalski, P., Reiss, K., Cheng, W., Cirielli, C., Kajstura, J., Nitahara, J.A., Rizk, M., Capogrossi, M.C., and Anversa, P. (1997). p53 Induces myocyte apoptosis via the activation of the renin-angiotensin system. Exp. Cell Res. *234*, 57–65.

Ravandi, F., Gojo, I., Patnaik, M.M., Minden, M.D., Kantarjian, H., Johnson-Levonas, A.O., Fancourt, C., Lam, R., Jones, M.B., Knox, C.D., et al. (2016). A phase I trial of the human double minute 2 inhibitor (MK-8242) in patients with refractory/recurrent acute myelogenous leukemia (AML). Leuk. Res. *48*, 92–100.

Riento, K., and Ridley, A.J. (2003). Rocks: multifunctional kinases in cell behaviour. Nat. Rev. Mol. Cell Biol. *4*, 446–456.

Saxton, R.A., and Sabatini, D.M. (2017). mTOR signaling in growth, metabolism, and disease. Cell *169*, 361–371.

Sohn, D., Graupner, V., Neise, D., Essmann, F., Schulze-Osthoff, K., and Janicke, R.U. (2009). Pifithrin-alpha protects against DNA damage-induced apoptosis downstream of mitochondria independent of p53. Cell Death Differ. *16*, 869–878.

Sullivan, K.D., Palaniappan, V.V., and Espinosa, J.M. (2015). ATM regulates cell fate choice upon p53 activation by modulating mitochondrial turnover and ROS levels. Cell Cycle *14*, 56–63.

Sumi, T., Matsumoto, K., Shibuya, A., and Nakamura, T. (2001). Activation of LIM kinases by myotonic dystrophy kinase-related Cdc42-binding kinase alpha. J. Biol. Chem. *276*, 23092–23096.

Takimoto, R., and El-Deiry, W.S. (2000). Wild-type p53 transactivates the KILLER/DR5 gene through an intronic sequence-specific DNA-binding site. Oncogene *19*, 1735–1743.

Tan, I., Ng, C.H., Lim, L., and Leung, T. (2001). Phosphorylation of a novel myosin binding subunit of protein phosphatase 1 reveals a conserved mechanism in the regulation of actin cytoskeleton. J. Biol. Chem. *276*, 21209–21216.

Tan, I., Yong, J., Dong, J.M., Lim, L., and Leung, T. (2008). A tripartite complex containing MRCK modulates lamellar actomyosin retrograde flow. Cell *135*, 123–136.

Tang, H.W., Wang, Y.B., Wang, S.L., Wu, M.H., Lin, S.Y., and Chen, G.C. (2011). Atg1-mediated myosin II activation regulates autophagosome formation during starvation-induced autophagy. EMBO J. *30*, 636–651.

Tasdemir, E., Chiara Maiuri, M., Morselli, E., Criollo, A., D'Amelio, M., Djavaheri-Mergny, M., Cecconi, F., Tavernarakis, N., and Kroemer, G. (2008a). A dual role of p53 in the control of autophagy. Autophagy *4*, 810–814.

Tasdemir, E., Maiuri, M.C., Galluzzi, L., Vitale, I., Djavaheri-Mergny, M., D'Amelio, M., Criollo, A., Morselli, E., Zhu, C., Harper, F., et al. (2008b). Regulation of autophagy by cytoplasmic p53. Nat. Cell Biol. *10*, 676–687.

Tasdemir, E., Maiuri, M.C., Orhon, I., Kepp, O., Morselli, E., Criollo, A., and Kroemer, G. (2008c).

p53 represses autophagy in a cell cycle-dependent fashion. Cell Cycle 7, 3006–3011.

Thornborrow, E.C., Patel, S., Mastropietro, A.E., Schwartzfarb, E.M., and Manfredi, J.J. (2002). A conserved intronic response element mediates direct p53-dependent transcriptional activation of both the human and murine bax genes. Oncogene 21, 990–999.

Tisato, V., Voltan, R., Gonelli, A., Secchiero, P., and Zauli, G. (2017). MDM2/X inhibitors under clinical evaluation: perspectives for the management of hematological malignancies and pediatric cancer. J. Hematol. Oncol. 10, 133.

Uehata, M., Ishizaki, T., Satoh, H., Ono, T., Kawahara, T., Morishita, T., Tamakawa, H., Yamagami, K., Inui, J., Maekawa, M., et al. (1997). Calcium sensitization of smooth muscle mediated by a Rho-associated protein kinase in hypertension. Nature 389, 990–994.

Unbekandt, M., Belshaw, S., Bower, J., Clarke, M., Cordes, J., Crighton, D., Croft, D.R., Drysdale, M.J., Garnett, M.J., Gill, K., et al. (2018). Discovery of potent and selective MRCK inhibitors with therapeutic effect on skin cancer. Cancer Res. 78, 2096–2114.

Unbekandt, M., Croft, D.R., Crighton, D., Mezna, M., McArthur, D., McConnell, P., Schuttelkopf, A.W., Belshaw, S., Pannifer, A., Sime, M., et al. (2014). A novel small-molecule MRCK inhibitor blocks cancer cell invasion. Cell Commun. Signal. 12, 54.

Unbekandt, M., and Olson, M.F. (2014). The actin-myosin regulatory MRCK kinases: regulation,

biological functions and associations with human cancer. J. Mol. Med. (Berl.) 92, 217–225.

van 't Veer, L.J., Dai, H., van de Vijver, M.J., He, Y.D., Hart, A.A., Mao, M., Peterse, H.L., van der Kooy, K., Marton, M.J., Witteveen, A.T., et al. (2002). Gene expression profiling predicts clinical outcome of breast cancer. Nature 415, 530–536.

van der Vos, K.E., Eliasson, P., Proikas-Cezanne, T., Vervoort, S.J., van Boxtel, R., Putker, M., van Zutphen, I.J., Mauthe, M., Zellmer, S., Pals, C., et al. (2012). Modulation of glutamine metabolism by the PI(3)K-PKB-FOXO network regulates autophagy. Nat. Cell Biol. 14, 829–837.

Vassilev, L.T., Vu, B.T., Graves, B., Carvajal, D., Podlaski, F., Filipovic, Z., Kong, N., Kammlott, U., Lukacs, C., Klein, C., et al. (2004). In vivo activation of the p53 pathway by small-molecule antagonists of MDM2. Science 303, 844–848.

Vousden, K.H., and Prives, C. (2009). Blinded by the light: the growing complexity of p53. Cell 137, 413–431.

Wagner, A.J., Banerji, U., Mahipal, A., Somaiah, N., Hirsch, H., Fancourt, C., Johnson-Levonas, A.O., Lam, R., Meister, A.K., Russo, G., et al. (2017). Phase I trial of the human double minute 2 inhibitor MK-8242 in PATIENTS WITH ADVANCED SOLID TUmors. J. Clin. Oncol. 35, 1304–1311.

Walton, M.I., Wilson, S.C., Hardcastle, I.R., Mirza, A.R., and Workman, P. (2005). An evaluation of the ability of pifithrin-alpha and -beta to inhibit p53 function in two wild-type p53 human tumor cell lines. Mol. Cancer Ther. 4, 1369–1377.

White, E. (2012). Deconvoluting the context-dependent role for autophagy in cancer. Nat. Rev. Cancer 12, 401–410.

Wilkinson, S., Paterson, H.F., and Marshall, C.J. (2005). Cdc42-MRCK and Rho-ROCK signalling cooperate in myosin phosphorylation and cell invasion. Nat. Cell Biol. 7, 255–261.

Wu, X., Bayle, J.H., Olson, D., and Levine, A.J. (1993). The p53-mdm-2 autoregulatory feedback loop. Genes Dev. 7, 1126–1132.

Yamamoto, A., Tagawa, Y., Yoshimori, T., Moriyama, Y., Masaki, R., and Tashiro, Y. (1998). Bafilomycin A1 prevents maturation of autophagic vacuoles by inhibiting fusion between autophagosomes and lysosomes in rat hepatoma cell line, H-4-II-E cells. Cell Struct. Funct. 23, 33–42.

Yang, S., Wang, X., Contino, G., Liesa, M., Sahin, E., Ying, H., Bause, A., Li, Y., Stommel, J.M., Dell'antonio, G., et al. (2011). Pancreatic cancers require autophagy for tumor growth. Genes Dev. 25, 717–729.

Yong, J., Tan, I., Lim, L., and Leung, T. (2006). Phosphorylation of myosin phosphatase targeting subunit 3 (MYPT3) and regulation of protein phosphatase 1 by protein kinase A. J. Biol. Chem. 281, 31202–31211.

Zhao, Z., and Manser, E. (2015). Myotonic dystrophy kinase-related Cdc42-binding kinases (MRCK), the ROCK-like effectors of Cdc42 and Rac1. Small GTPases 6, 81–88.

Supplemental Information

Identification of Kinases Responsible

for p53-Dependent Autophagy

Stephanie L. Celano, Lisette P. Yco, Matthew G. Kortus, Abigail R. Solitro, Hakan Gunaydin, Mark Scott, Edward Spooner, Ronan C. O'Hagan, Peter Fuller, Katie R. Martin, Stuart D. Shumway, and Jeffrey P. MacKeigan
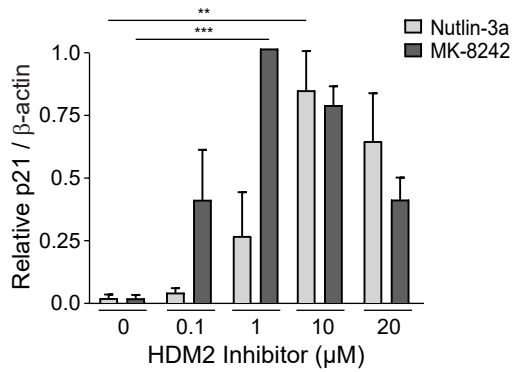
Figure S1

Figure S1. MK-8242 has a lower effective concentration compared to Nutlin-3a, Related to Figure 1. U2OS cells were treated as in Figure 1A and lysates probed for p21 and β-actin. The relative p21 signal was determined by dividing p21 band intensity by the corresponding β-actin band intensity (normalized to 1.0 for 1μM MK-8242). Bars represent the mean of 3 biological experiments and error bars represent SEM. Two-Way ANOVA, Tukey multiple comparison test: **$p < 0.01$, ***$p < 0.001$.
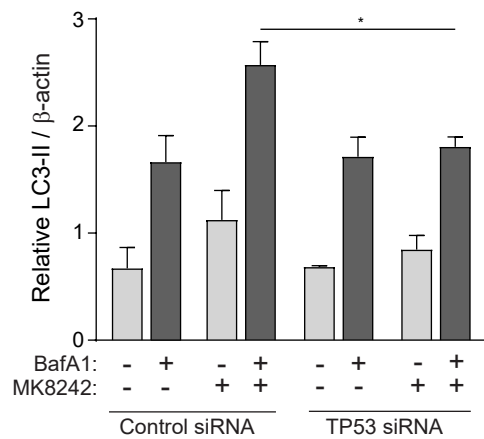
Figure S2

Figure S2. MK-8242 induced autophagy is p53-dependent, Related to Figure 2.
U2OS cells were treated as in Figure 2E and lysates probed for LC3-II and β-actin. Relative LC3-II signal was determined by dividing LC3-II band intensity by the corresponding β-actin band intensity. Bars represent the mean of 2 biological experiments and error bars represent SD. Two-Way ANOVA, Tukey multiple comparison test, *p<0.05.
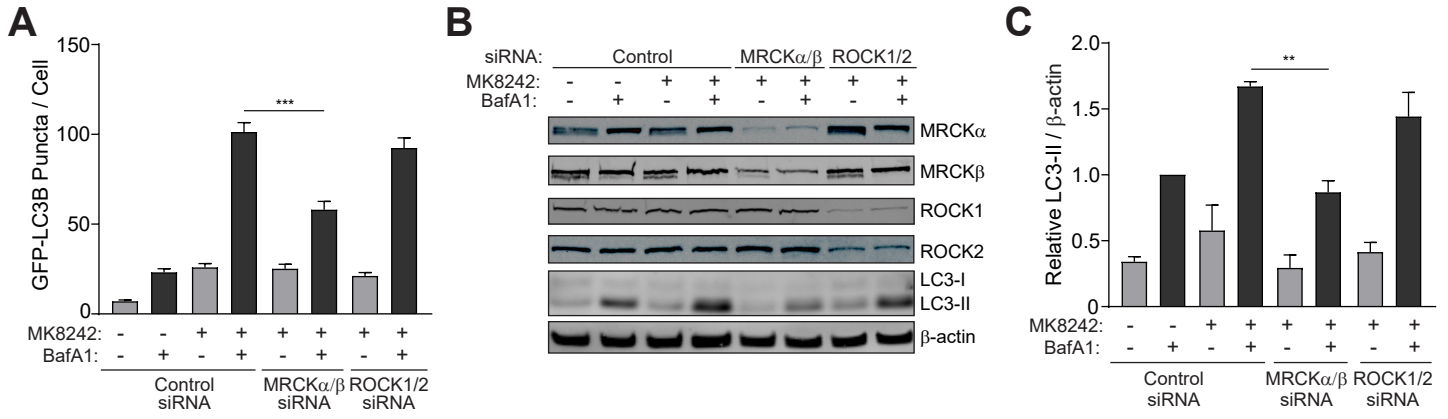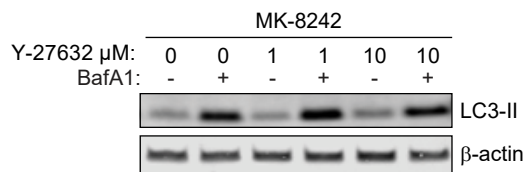
Figure S3

Figure S3. MRCKα/MRCKβ, not ROCK1/ROCK2, selectively suppresses p53-mediated autophagy, Related to Figure 4. (A) U2OS-EGFP-LC3B cells were treated with indicated siRNAs for 24 hours, with (+) or without (-) 1 μM MK-8242 for an additional 24 hours and, with (+) or without (-) 100 nM BafA1 for the final 1.5 hours for a total treatment time of 48 hours. The number of EGFP-LC3B puncta quantified (≥ 60 cells per condition). Bars represent means of all cells and error bars represent SEM. Two-Way ANOVA, Tukey multiple comparison test: ***p<0.001. (B) U2OS cells were treated with the indicated siRNAs for 24 hours, with (+) or without (-) 1 μM of MK-8242 for an additional 24 hours and, with (+) or without (-) 100 nM BafA1 for the final 1.5 hours for a total treatment time of 48 hours. Lysates were probed for MRCKα, MRCKβ, ROCK1, ROCK2, LC3-II, and β-actin. (C) Relative LC3-II signal from (B) was determined by dividing LC3-II band intensity by the corresponding β-actin band intensity (normalized to 1.0 for the vehicle (+) BafA1 control). Bars represent the mean of 3 biological replicates and error bars represent SEM. Two-Way ANOVA, Tukey multiple comparison test: **p<0.01.

Figure S4

A

MK-8242

Y-27632 µM:	0	0	1	1	10	10
BafA1:	-	+	-	+	-	+

LC3-II

β-actin

B

MK-8242

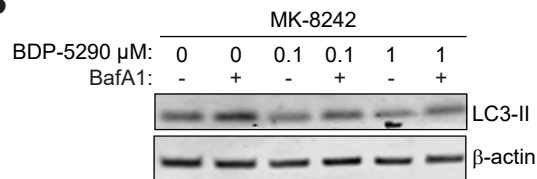| BDP-5290 µM:	0	0	0.1	0.1	1	1
BafA1:	-	+	-	+	-	+

LC3-II

β-actin

Figure S4. MRCK inhibition, not ROCK inhibition, suppresses p53-mediated autophagy, Related to Figure 4. (A) U2OS cells were treated with the indicated doses (0, 1, or 10 µM Y-27632) and 1 µM MK-8242 for 24 hours, with (+) or without (-) BafA1 for the final 1.5 hours for a total treatment time of 24 hours. Lysates were probed for LC3-II and β-actin. (B) U2OS cells were treated with the indicated doses (0, 0.1, or 1 µM BDP-5290) and 1 µM MK-8242 for 24 hours, with (+) or without (-) BafA1 for the final 1.5 hours for a total treatment time of 24 hours. Lysates probed for LC3-II and β-actin.
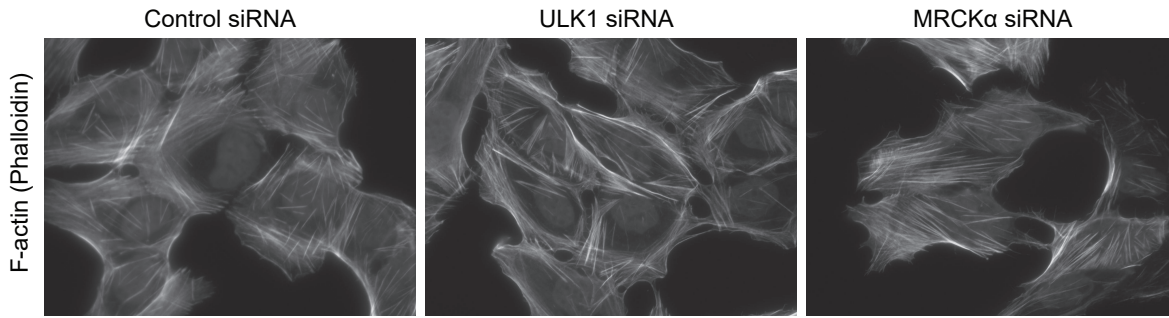
Figure S5

Figure S5. Change in actin network and well-aligned stress fibers in MRCKα knockdown cells, Related to Figure 5. U2OS cells were treated with the indicated siRNAs for 48 hours, cells stained for F-actin (phalloidin) and, nuclei counterstained. Merged grayscale image shown.

siRNA:	Control	Control	*TP53*	*TP53*	Control	*TP53*
Treatment:	Control	MK-8242	Control	MK-8242	MK-8242	MK-8242
TARGET					% increase	% remaining
CDKN1A	392	3270	217	664	834	20
BAX	54	347	41	79	639	23
GADD45A	32	238	21	70	748	30
MDM2	3	74	3	20	2123	27
TNFRSF10B	11	60	9	16	553	26

Table S1. MK-8242 effects on p53 target genes, Related to Figure 1. qRT-PCR was performed on RNA isolated from cells transfected with control or *TP53* siRNAs and treated with or without MK-8242. Relative copy numbers (*10,000) were calculated by dividing the average Ct values of target genes by the average Ct value of houskeeping reference genes (*ACTB, B2M*, *GAPDH*, and *RPLP0*). The increase (%) in expression with MK-8242 treatment and remaining (%) following *TP53* knockdown for each taget gene are shown.

siRNA:	Control	Control	Control	TP53	TP53	TP53	Control	TP53	Control	TP53
Treatment:	Control	Nutlin-3a	MK-8242	Control	Nutlin-3a	MK-8242	Nutlin-3a	Nutlin-3a	MK-8242	MK-8242
TARGET							% increase	% remaining	% increase	% remaining
DRAM1	669	8698	8950	712	1858	2062	1301	21	1339	23
SESN2	453	6717	7392	414	1024	1760	1482	15	1631	24
ATG4A	240	965	1160	365	559	635	403	58	484	55
FOXO3A	219	864	887	169	219	431	395	25	406	49

Table S2. Effect of HDM2 inhibition on p53 target autophagy-related genes, Related to Figure 1.
qRT-PCR was performed on RNA isolated from cells transfected with control or *TP53* siRNAs and treated with vehicle control, 10 μM Nutlin-3a, or 1 μM MK-8242. Relative copy numbers (*10,000) were calculated by dividing the average Ct value of target genes by the average Ct value of housekeeping reference gene (*HPRT1*). The increase (%) expression with Nutlin-3a or MK-8242 treatment and remaining (%) following *TP53* knockdown for each target gene are shown.

TRANSPARENT METHODS

Mammalian cell culture, reagents, and antibodies
The human osteosarcoma cell line U2OS (HTB-96) was purchased from American Type Culture Collection, and cells maintained in McCoy's 5A medium (Gibco, 16600-082) supplemented with 10% fetal bovine serum (Corning, 35-010-CV) and cultured at 37°C in a humidified atmosphere containing 5% CO_2. Cells were seeded 24 hours before the start of assays. Nutlin-3a (Selleck Chemicals, S1061), MK-8242 (Merck & Co., Inc.), rapamycin (Millipore-Sigma, 553210), Y-27632 (Tocris, 1254), BDP-5290 (Aobious, AOB6539), and Bafilomycin A1 (BafA1; AG Scientific, B1183) stock solutions were prepared in dimethyl sulfoxide (DMSO) (Sigma-Aldrich, D2650). Equal concentrations of DMSO used for control treatments. Primary antibodies used were LC3B (Sigma-Aldrich, L7543), p21 Waf1/Cip1 (Cell Signaling Technology, 2947), p53 (Cell Signaling Technology, 2527), ROCK1 (Cell Signaling Technology, 4035), ROCK2 (Cell Signaling Technology, 8236), MRCKα (Santa Cruz Biotechnology, sc-374568), MRCKβ (Santa Cruz Biotechnology, sc-374597), β-actin (Cell Signaling Technology, 3700). Horseradish peroxide (HRP)-conjugated secondary anti-mouse (NA931V), and anti-rabbit (NAV934V) purchased from GE Healthcare Life Sciences. IRDye infrared fluorescent 800CW secondary goat anti-rabbit (926-32211) and anti-mouse (926-32210), and 680RD secondary goat anti-rabbit (926-68071) and anti-mouse (926-68070) purchased from LI-COR.

Immunoblot analysis
Cell lysates were prepared in ice-cold lysis buffer [10mM potassium phosphate, 1 mM ethylenediaminetetraaceticacid (EDTA), 10 mM magnesium chloride, 5 mM ethylene-bis(oxyethylenenitrilo)tetraacetic acid (EGTA), 50 mM bis-glycerophosphate, 0.5% Nonidet P-40 (NP-40), 0.1% Brij35, 0.1% sodium deoxycholate, 2 mM dithiothreitol, 1 mM sodium orthovanadate, 5 mM sodium fluoride, and protease inhibitor cocktail (Sigma-Aldrich, P8340)]. Lysate samples were clarified by centrifugation for 10 min at 13,000 rpm and 4°C. Total protein concentration was determined using Protein Assay Dye Reagent Concentrate (Bio-Rad, 5000006). Proteins resolved by SDS-polyacrylamide gel or pre-cast 4-12% BOLT Bis-Tris Plus gels (Invitrogen, NW04125BOX) and electrotransferred onto either nitrocellulose or polyvinylidene difluoride membranes. Membranes blocked with 5% nonfat dry milk in 1X Tris-buffered saline and 0.1% Tween-20 (0.1% T-TBS) or StartingBlock (TBS) Blocking Buffer (Thermo Scientific, 37542) followed by overnight incubation of primary antibodies diluted in 5% BSA, 0.1% T-TBS or StartingBlock T20 (TBS) Blocking Buffer (Thermo, 37543) at 4°C. After three 5 min 0.1% T-TBS washes, membranes incubated in secondary antibodies diluted in 5% milk blocking buffer or StartingBlock T20 (TBS) Blocking Buffer for 1 hour at room temperature. Protein bands detected by enhanced chemiluminescence, West Femto Maximum Sensitivity Substrate (Thermo, 34095), or imaged using LI-COR Odyssey Infrared Imaging System and quantified with LI-COR Image Studio Software.

Knockdown of target genes by siRNA
The following Flexitube siRNAs were purchased from Qiagen: Hs_TP53 siRNA8 and 13 (SI02623754, SI04384079), Hs_ULK1 siRNA5 and 6 (SI02223270, SI02223277), Hs_CDC42BPA siRNA6 and 8 (SI00287448, SI02631419), Hs_CDC42BPB siRNA4 and

6 (SI00083930, SI02622186), Hs_ROCK1 siRNA9 and 10 (SI02622095, SI02622102), and Hs_ROCK2 siRNA5 and 6 (SI02223746, SI02223753). U2OS cells seeded in 10 cm culture plates (4.0 x 10^5 cells per plate) or 6-well culture plates (3.0 x 10^4 cells per well). The next day, cells transfected with siRNAs (two independent sequences per target gene) targeting ULK1, MRCKα (CDC42BPA), MRCKβ (CDC42BPB), ROCK1, ROCK2 or combination MRCKα/MRCKβ and ROCK1/ROCK2 pool siRNAs using Oligofectamine (Invitrogen, 12252011) for 48 h. AllStars Negative Control siRNA (Qiagen, SI03650318) used as a control siRNA.

Purification of nuclear extracts

Purification of nuclear extracts from U2OS cells treated with Nutlin-3a (10 μM) or MK-8242 (1 μM, 10 μM) for 24 h was carried out with a Nuclear Extraction Kit (Cayman, 10009277), following the manufacturer's protocol. Briefly, treated cells were collected and washed using ice-cold 1X PBS/phosphatase inhibitor solution. Cells were pelleted by centrifugation (300 x g) for 5 min at 4°C. Pellets were resuspended in ice-cold complete hypotonic buffer and allowed to swell for 15 min. NP-40 assay reagent was mixed into the samples and centrifuged (14,000 x g) for 30 sec at 4°C. The supernatant which contains the cytosolic fraction stored at -80°C. Nuclear pellets resuspended by a vortex in ice-cold complete nuclear extraction buffer and centrifuged (14,000 x g) for 30 sec at 4°C, saving the supernatant (i.e., nuclear cell extract). Protein concentrations were determined using Bio-Rad Protein Assay Dye Reagent.

Nuclear p53 DNA binding activity

p53 DNA binding activity was detected using a p53 assay DNA-binding enzyme-linked immunosorbent assay (ELISA) (Cayman, 600020), following the manufacturer's protocol. Specific double-stranded DNA (dsDNA) sequences containing p53 response elements bound onto each well of a 96-well plate. In brief, equal amounts of nuclear extracts and controls were added to each well and incubated for 1 h at room temperature. After incubation, wells washed with wash buffer. p53 primary antibody (Cayman, 600023) was added to each well, excluding blank control wells, and incubated for 1 h at room temperature without agitation. Wells were washed and incubated with diluted goat anti-mouse HRP conjugate. After 1 h incubation at room temperature, wells were washed and incubated with the developing solution for 15-45 min at room temperature with gentle agitation and protected from light. Stop solution added in each well and absorbance measured at 450 nm.

Fluorescence microscopy and vesicle quantification

A monoclonal U2OS cell line was generated that expresses the ptfLC3B plasmid, a gift from Tamotsu Yoshimori (Addgene plasmid 21074) (Kimura et al., 2007). U2OS-ptfLC3B cells (2.0 x 10^4 cells per well) were seeded in 24-well tissue culture plates on number 1.5 coverglass and allowed to settle for 24 h. Cells were transfected with siRNA target genes and siRNA control. Twenty-four hours post-transfection, cells treated with MK-8242 for another 24 h or rapamycin, 46 h post transfection, for 2 h with addition of 100 nM BafA1 for the last 1.5 h. For Figure 5 a monoclonal U2OS cell line was generated with low expression of the pMXs-puro-GFP-DFCP1 plasmid, a gift from Noboru Mizushima (Addgene plasmid 38269). U2OS-GFP-DFCP1 cells (2.0 x 10^4 cells per well) were

seeded in 24-well tissue culture plates on number 1.5 coverglass and allowed to settle for 24 h. Cells were transfected with siRNA target genes and siRNA control. Twenty-four hours post-transfection, cells were treated with 1 µM MK-8242 for another 24 hours. Equal concentrations of DMSO used for vehicle controls. For Figure S5 U2OS-WT cells ($4.0\text{x}10^3$ cells per well) were seeded in a 96 well glass bottom plate and allowed to settle for 24 h. Cells transfected with siRNA target genes and siRNA control for 48 hours. After treatments, U2OS-ptfLC3B, U2OS-GFP-DFCP1, or U2OS-WT cells were fixed in 4% formaldehyde (Pierce/Thermo, 28908), washed with DPBS (Thermo, 14190250), and stained with Hoechst nuclear stain (Invitrogen, H1399). In Figure S5, cells were then permeabilized with 0.02% Triton-X 100 DPBS, blocked in 3% BSA in DPBS, and stained with Alexa Fluor 488 Phalloidin (Invitrogen, A12379). All coverslips were mounted onto slides using Fluoro-Gel (Electron Microscopy Sciences, 17985-10). Cells were imaged using a 60X oil objective, in FITC and DAPI channels, on a Nikon Ti Eclipse fluorescent microscope. U2OS-ptfLC3B and U2OS-GFP-DFCP1 images were deconvolved, top-hat transformed (peak identification), and thresholded (intensity) using NIS Elements Software to quantify EGFP-LC3-positive or GFP-DFCP1-positive puncta per cell (Martin et al., 2013).

p53 target gene expression
Total RNA was extracted from U2OS cells using the RNeasy Mini Kit (Qiagen, 74104) and Qiashredder kit (Qiagen, 79654). cDNA was synthesized using an iScript Select cDNA Synthesis Kit (Bio-Rad, 170-8896) and diluted in TE (Tris-EDTA) buffer. Synthesized cDNA samples were mixed with Applied Biosystems Fast SYBR Green Master Mix (Thermo, 4385612). Quantitative real-time PCR was performed using Applied Biosystems 7500 and ViiA7 Real-Time PCR Systems. RT² qPCR Primer Assays for human *CDKN1A* (Qiagen, PPH00211E), *BAX* (Qiagen, PPH00078B), *GADD45A* (Qiagen, PPH00148B), *MDM2* (Qiagen, PPH00193E), and *TNFRSF10B* (Qiagen, PPH00241C) were used to measure p53 target gene expression following MK-8242 treatment. Primers for human *DRAM1* (fwd: CGGATGGTCATCTCTGCCGTTT, rev: CTGTCCATTCACAGATCGCACTC), *SESN2* (fwd: AGATGGAGAGCCGCTTTGAGCT, rev:CCGAGTGAAGTCCTCATATCCG),*ATG4A*(fwd:CCAAGCCAGAAGTGACAACCAC, rev:GACAGACCTTCAAGTTGAGTTCC),and*FOXO3A*(fwd:TCTACGAGTGGATGGTGC GTTG, rev: CTCTTGCCAGTTCCCTCATTCTG) were used to measure the autophagy-related p53 target genes in response to MK-8242 and Nutlin-3a treatment. Human *HPRT1* (fwd:ATGGACAGGACTGAACGTCTTGCT,rev:GCTTTGATGTAATCCAGCAGGTCAGC) was used as a reference gene.

Confocal microscopy-based human kinase screen
U2OS-ptfLC3B cells (4.5×10^3 cells per well) were seeded in 96-well glass bottom plates, and cells transfected with siRNA pools (four independent sequences per target gene, human kinase siRNA library version 2.0, Qiagen) and siRNA controls. Cells were transfected at a final concentration of 25 nM using 0.2 µl Oligofectamine (Invitrogen #12252-011) transfection reagent per well. A total of 748 gene targets, as well as positive control (ATG5/ATG12 and ATG9A/ATG9B) siRNAs, were screened in sixteen 96-well plates. Twenty hours post-transfection, cells were treated with 10 µM MK-8242 for 24 h with addition of BafA1 for the last hour. After treatments, cells were washed with PBS,

permeabilized with 0.02% Digitonin (Sigma-Aldrich, D141), and fixed with 2% formaldehyde. Cell nuclei were stained using Hoechst and mounted using Fluoro-Gel (Electron Microscopy Sciences, 17985-10). U2OS-ptfLC3B cells were imaged using 20X objective, in 403 and 488 nm excitation lasers, on a Nikon A1 confocal microscope. Five z-planes with 4 micron intervals captured in two adjacent fields of view. Z-planes combined into a maximum intensity projection, and autophagy quantified by calculating the object intensity per cell (the measured total fluorescence intensity of EGFP-LC3B divided by the number of nuclei within a field of view).

Statistical Analysis

All statistical tests performed in GraphPad Prism with statistical significance defined as $p \leq 0.05$. Two-Way ANOVA with Tukey multiple comparison tests used for all analysis. Biological replicates and error bars represent standard error of the mean (SEM), unless otherwise indicated. *$p < 0.05$, **$p < 0.01$, ***$p < 0.01$. In Figure 3 and Table S3, the siRNAs were sorted by standard deviations from plate-normalized means.